Journal Pre-proof

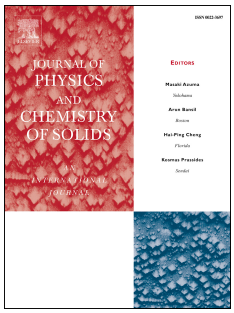

Structural, morphological and dielectric properties of $ErNbO_4$ prepared by the sol-gel method

S. Devesa, S. Soreto Teixeira, A.P. Rooney, M.P. Graça, D. Cooper, L.C. Costa

PII: S0022-3697(20)30800-3

DOI: https://doi.org/10.1016/j.jpcs.2020.109619

Reference: PCS 109619

To appear in: *Journal of Physics and Chemistry of Solids*

Received Date: 25 March 2020

Revised Date: 10 May 2020

Accepted Date: 8 June 2020

Please cite this article as: S. Devesa, S.S. Teixeira, A.P. Rooney, M.P. Graça, D. Cooper, L.C. Costa, Structural, morphological and dielectric properties of $ErNbO_4$ prepared by the sol-gel method, *Journal of Physics and Chemistry of Solids* (2020), doi: https://doi.org/10.1016/j.jpcs.2020.109619.

Author statement

Susana Devesa: Conceptualization, Methodology, Investigation, Writing - Original Draft, Validation, Formal analysis, Data curation, Visualization.

Sílvia S. Teixeira: Investigation, Writing - Original Draft, Validation

Aidan P. Rooney: Investigation, Writing - Original Draft

Manuel P. Graça: Writing - Review & Editing

David Cooper: Writing - Review & Editing

Luís C. Costa: Writing - Review & Editing, Supervision

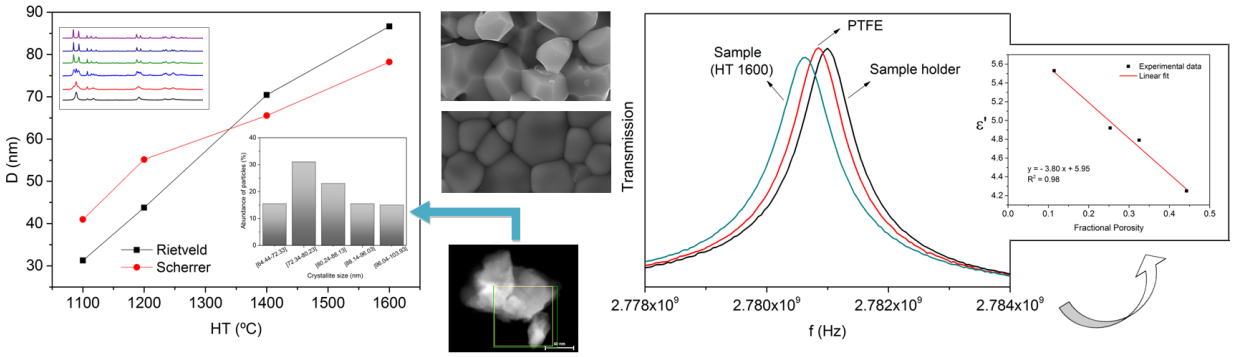

Structural, morphological and dielectric properties of $ErNbO_4$ prepared by the sol-gel method

S. Devesa[a,b*], S. Soreto Teixeira[b], A.P. Rooney[c], M. P. Graça[b], D. Cooper[c], L. C. Costa[b]

[a] CFisUC, Physics Department, University of Coimbra, Rua Larga, 3004-516 Coimbra, Portugal
[b] I3N and Physics Department, University of Aveiro, 3810-193 Aveiro, Portugal
[c] CEA LETI-Minatec, 17 Rue des Martyrs, 38054 Grenoble Cedex 9, France
* Corresponding author: susana_devesa@hotmail.com

Abstract

In this work, $ErNbO_4$ samples were prepared using the sol-gel method, through the citrate route, and heat-treated at temperatures between 700 and 1600 ºC. The structure was studied by X-ray diffraction and Raman spectroscopy. The crystallite size was estimated using the Rietveld refinement and the Sherrer's formula, presenting values from 31.27 to 86.65 nm and from 40.96 to 78.23 nm, respectively. The morphology was studied by scanning electron microscopy. The measurement of the complex permittivity was made using the small perturbation technique, with a cavity operating in TE_{105} mode, at resonant frequency of 2.7 GHz. The increase of the treatment temperature promoted the increase of the dielectric constant and the dielectric losses were still maintained with low values, allowing their potential application in electric storage devices. The dielectric constant of $ErNbO_4$ in a zero porosity sample case was estimated and compared with the experimental values.

***Keywords*:** Ceramics; sol-gel; rare-earth orthoniobates; microwave; dielectric properties.

1 Introduction

In the last two decades, the microwave frequency region has been adopted in the civilian electronic communication system. Consequently, that allows the development of new dielectric materials, with the reduction of size and weight of electronic components becoming a priority [1-3].

In this context, the ABO_4 ternary oxides have been studied since their ability to combine chemical elements in this basic formula leads to a large number of structures and phases with different properties, such as $BiNbO_4$ or $Bi(Sb,Nb,Ta)O_4$ [4-7]. A special interest appears in the rare-earth orthoniobates, $RENbO_4$, which belongs to the family of $A^{3+}B^{5+}O_4$ compounds. Recently, properties such as mixed protonic, native ionic and electronic conductive properties, are being studied [6,8].

The conventional solid state method is the most used ones for the preparation of oxides, and the ABO_4 compounds are no exception [9]. ABO_4 oxides can be prepared by the solid state reaction method, resulting in powders with high crystallinity, but not always in pure and homogeneous phases, since metastable phases can be formed under these conditions [6]. Other disadvantages documented in the literature are: large grain growth, segregation of components and loss of stoichiometry [9,10,11,12].

Some alternative methods have been investigated to prepare oxides, namely wet-chemical techniques, such as sol-gel citrate, co-precipitation, hydrothermal and combustion syntheses. These methods can be considered advantageous since they produce oxides with nanosized particles (thus, high surface area), high reactivity and very good homogeneity. Among these routes, the sol-gel citrate method has been considered a simple way to obtain stable precursors and stoichiometric fine powders. This method is considered suitable to achieve high homogeneity at relatively low temperature, since the formation of citrate complexes allows mixing the precursors cations on an atomic scale, and consequently, they can react with each other immediately [9–14].

The functionality of a dielectric ceramic is mainly determined by its electrical properties, namely their dielectric constant, ε', and dielectric losses, ε'', values [3,15]. For example, a ceramic material with low losses and with ε' in the range of 4-12, at room temperature and in the GHz range, can be used for millimeter wave communication systems and, also, as substrates for microwave integrated circuits [16].

The $RENbO_4$ are an interesting group of materials due to the complexity of their structure and properties, making them eligible for a variety of applications. The complexity arises mainly from the range of possible coordination of the Nb cation, from 8 to 4 [17].

The structure of the monoclinic $ErNbO_4$ consists of ErO_8 dodecahedrons and NbO_4 tetrahedrons. While the known structures are dominated by pentavalent Nb atoms in octahedral coordination, rare-earth niobate fergusonites, such as $ErNbO_4$, and scheelites, are exceptions. These structures are seen as one of the enigmas of crystal chemistry [17,18] and might play an important role in the dielectric properties of this class of materials.

In this work, $ErNbO_4$ powders were prepared using the sol-gel method and their dielectric properties were studied at 2.7 GHz using the small perturbation method.

Since it is known that the behaviour of functional materials is intrinsically related with their structures [19], structural characterization of the obtained powders was performed, using X-ray diffraction and Raman scattering.

2 Experimental methods

$ErNbO_4$ powders were prepared using the sol-gel method, through the citrate route.

A suspension containing stoichiometric amounts of $Er(NO_3)_3 \cdot 5H_2O$ (99%, Aldrich) and $NbCl_5$ (99%, Merck) was initially prepared in a minor amount of hydrogen peroxide (3% V/V) and dispersed in a mixture of citric acid and ethylene glycol (Sigma-Aldrich), used as chelating agent and reaction medium, respectively. To promote the solubility, the suspension was stirred for 7 days until a clear colloidal suspension was formed. Subsequent to that, the solution was dried at 500 °C for 6 h to evaporate the solvent. The obtained powders were pressed into cylinders, of 4 mm in diameter and 10 mm in height, and were heat-treated at 700, 800, 900, 1100, 1200, 1400 and 1600 ºC for 4 h. The heating rate of 5 ºC/min was used and the cooling process was made naturally.

The structural characterization was performed using X-ray diffraction (XRD). The patterns were obtained on an Empyrean diffractometer (CuK α radiation, λ=1.54060 Å) at 45 kV and 40 mA, in a Bragg-Brentano parafocusing optics configuration. Intensity data was collected by the step counting method (step 0.02 º in 1 s) in the 2θ angle range of 10-60 º.

For the sample with the most promising dielectric properties, a TEM specimen was prepared by dropcasting a suspension of ground powder and ethanol onto a holey carbon TEM grid. STEM characterization was performed in a probe-side aberration-corrected FEI Titan Themis S/TEM with a 200kV 150 pA electron beam. Both bright field and high angle annular dark field (HAADF) detectors were used to identify the particles as crystalline and characterize their morphology and size. Energy dispersive X-ray (EDX) spectrum imaging was acquired in parallel. The relative intensities of the erbium, niobium and oxygen characteristic edges were used to map the distribution of these elements across the particles.

The Micro-Raman spectra were recorded at room temperature, with a HR-800-UV Jobin Yvon Horiba spectrometer, in backscattering geometry with a 441.6 nm laser line.

The morphology of the samples was analyzed by scanning electron microscopy (SEM). The images were obtained on a TESCAN-Vega III, on the free and fractured surfaces. Previous to the microscopic observation, the samples were covered with carbon.

The measurements of the complex permittivity were made at 2.7 GHz, in a resonant cavity operating in the TE_{105} mode, coupled to a HP 8753D Network Analyzer.

Introducing a sample in the centre of the cavity, where the electric field is maximal, the changes in the resonant frequency, Δf, and in the inverse of the quality factor $\Delta(1/Q)$ of the resonant cavity can be related with the permittivity values, [1,19]. The shift in the resonant frequency of the cavity can be related to the real part of the complex permittivity, ε', and the change in the inverse of the quality factor of the cavity can be related with the imaginary part, ε''.

Using the small perturbation technique and considering only the first order perturbation in the electric field caused by the sample [20], the real, ε', and the imaginary parts, ε'', of the complex permittivity were calculated using Eqs. (1) and (2)

$$\varepsilon' = K\frac{\Delta f}{f_0}\frac{V}{v} + 1 \quad (1)$$

$$\varepsilon'' = \frac{K}{2}\Delta\left(\frac{1}{Q}\right)\frac{V}{v} \quad (2)$$

K is a constant related to the depolarization factor, which depends upon the geometric parameters, v and V are the volumes of the cylindrical sample and the cavity, respectively, and f_0 is the resonance frequency of the cavity. Using a sample of known dielectric constant, in this study polytetrafluorethylene (PTFE), the constant K can be determined, and consequently, ε' and ε'' calculated.

3 Results and discussion

The XRD patterns of the prepared samples are shown in Figure 1(a). For heat treatments below 1100 ºC, besides the $ErNbO_4$ phase, the secondary phase $Er_{0.5}Nb_{0.5}O_2$ (tetragonal) was identified. Above 1100 ºC, all the detectable peaks were indexed only to $ErNbO_4$ monoclinic structure found in the standard reference data [21].

The Rietveld refinements simulations, made for the samples with single $ErNbO_4$ phase, allowed the estimation of the lattice parameters, typical crystallite sizes, D, and the strain induced in powders due to crystal imperfections and distortion, ε_s, which are assembled in Table I.

Figure 1 (b) shows the measured and the calculated spectra for the sample treated at 1100 ºC. Consistent results were obtained from the Rietveld refinements, with $R_{exp} \leq R_p$ and $\chi^2 > 1$ [22], which shows the good quality of the fitting,

Table I also shows the crystallite size determined using the Scherrer's formula, which will be approached later.

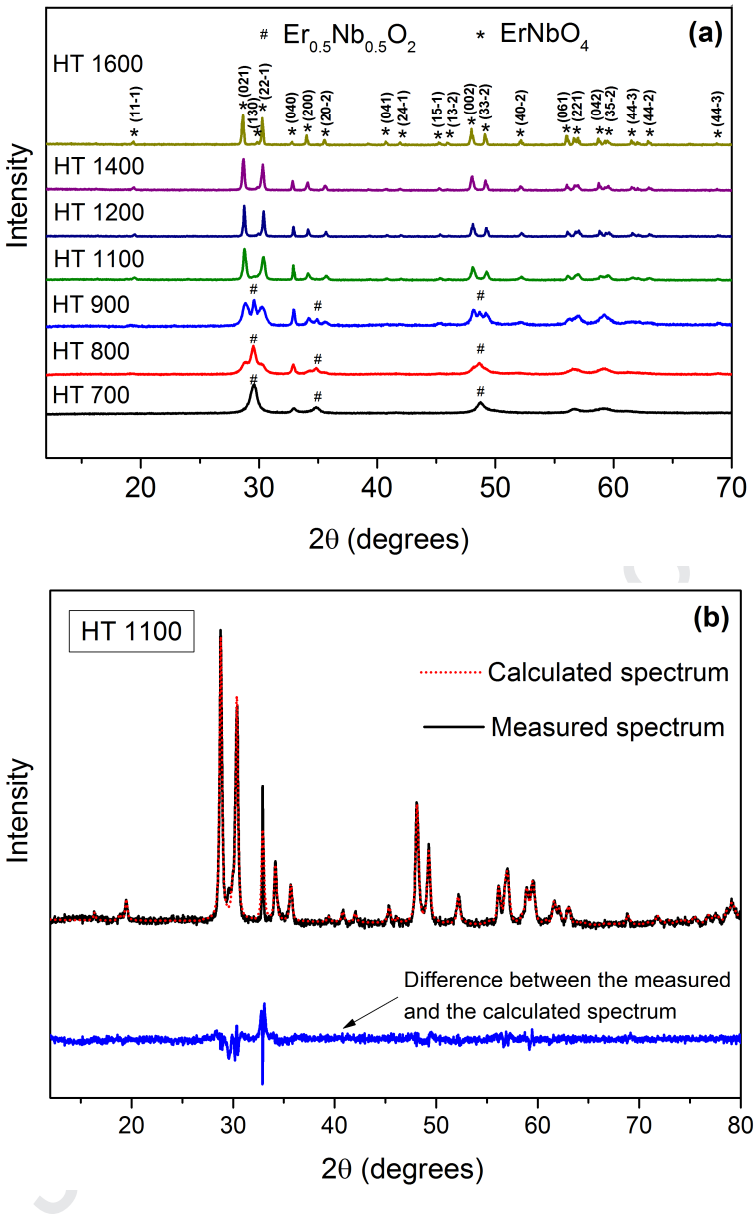

Figure 1 – (a) X-ray diffraction patterns of the prepared powders; **(b)** Measured and calculated spectra of the sample treated at 1100 ºC .

Table I - Rietveld fitting parameters, diffraction pattern fitting factors and crystallite size calculated from Scherrer's formula.

Temperature (ºC)	**Lattice parameters (nm)**	**β (º)**	**$D_{Rietveld}$ (nm)**	**ε_s ($\times 10^{-3}$)**	**R-factor**	**χ^2**	**$D_{Scherrer}$ (nm)**
1100	a = 0.7031 b = 1.0916 c = 0.5062	131.52	31.27	2.7	R_p = 5.03 R_{wp} = 7.17 R_{exp} = 3.89	3.39	40.96
1200	a = 0.7024 b = 1.0914 c = 0.5062	131.48	43.75	1.9	R_p = 4.89 R_{wp} = 6.57 R_{exp} =4.26	2.37	55.17
1400	a = 0.7024 b = 1.0917 c = 0.5064	131.46	70.43	1.2	R_p = 5.15 R_{wp} = 6.65 R_{exp} = 4.68	2.02	65.55
1600	a = 0.7022 b = 1.0911 c = 0.5064	131.42	86.65	1.0	R_p = 5.40 R_{wp} = 7.03 R_{exp} = 5.19	1.83	78.23

The most important properties that can be extracted from peak width analysis are the crystallite size, a measure of the size of coherently diffracting domains, and the lattice strain, a measure of the distribution of lattice constants arising from crystal imperfections, such as lattice dislocations, which affect the Bragg peak in different ways. These effects increase the peak width and intensity and shift the 2θ peak position accordingly [23,24]. Figure 2 shows, for the samples with single $ErNbO_4$ phase, the relation between the crystallite size and the lattice strain estimated through the Rietveld analysis. As one can see, the crystallite size of $ErNbO_4$ increases with the increase of the treatment temperature, with the lattice strain showing the opposite trend. This tendency can be due to the decrease of the number of boundaries with the increase of the crystallite size, since one of the sources of lattice strain is the crystal boundary triple junction [23,24].

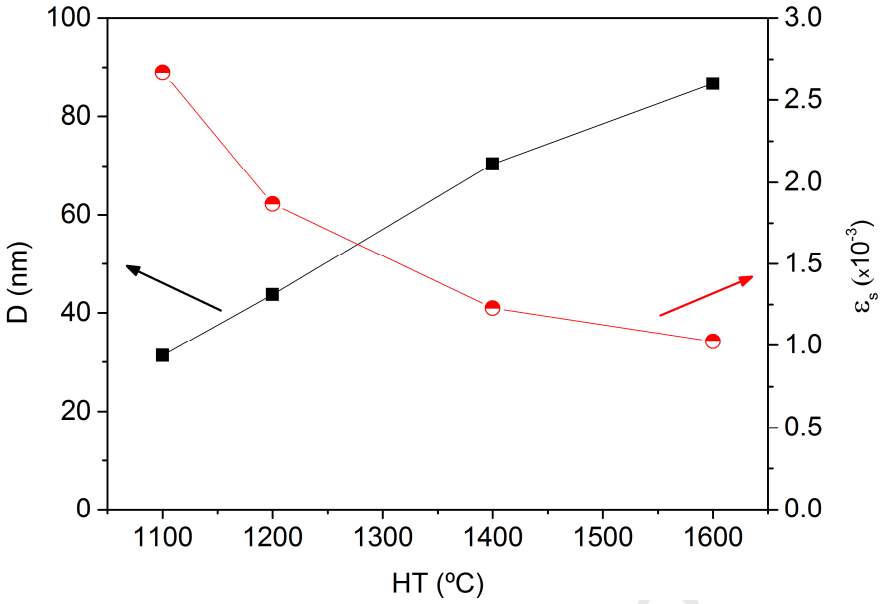

Figure 2 - Heat treatment dependence of the crystallite size and the lattice strain estimated through the Rietveld analysis.

The $ErNbO_4$ crystallite size for the samples treated above 1100 ºC was also calculated using the standard Scherrer's formula (Table I)

$$D = \frac{N\lambda}{\beta\cos\theta} \tag{3}$$

where λ is the wavelength of X-ray radiation, β is full width half maximum of the diffracted peaks, θ is the angle of diffraction and N is a numerical factor, often referred as the crystallite-shape factor [25,26]. According to the literature, N = 0.89 is considered a suitable approximation [27,28].

The β parameter was corrected using the equation

$$\beta = \sqrt{W_{exp}{}^2 - W_{inst}{}^2} \tag{4}$$

where w_{exp}, w_{inst} are the experimental and instrumental width, respectively. The instrumental width was obtained with the LaB_6 (SRM 660 - National Institute of Standard Technology) powder standard pattern [29].

By substituting the relevant data from XRD profile measurement, the average crystallite size was found to be between 40.96 and 78.23 nm.

As presented in figure 3, one can see a good agreement between the Rietveld and the Scherrer's formula, with the bigger crystallite size occurring for the sample treated at 1600 ºC. For the samples heat-treated at 1100 and 1200 ºC, the ones with higher lattice strain, the crystallite sizes obtained by Scherrer's formula are slightly higher than those obtained earlier by the Rietveld

analysis. This difference may be due to the fact that the effect of the internal strain is not considered in the Scherrer's model, where the peak shape is fitted with a Gaussian function only. However, in the Rietveld method, the peaks shape profile is fitted using a Voight function, which is a combination of both Gaussian (crystallite size) and a Lorentzian (microstrain) functions [30].

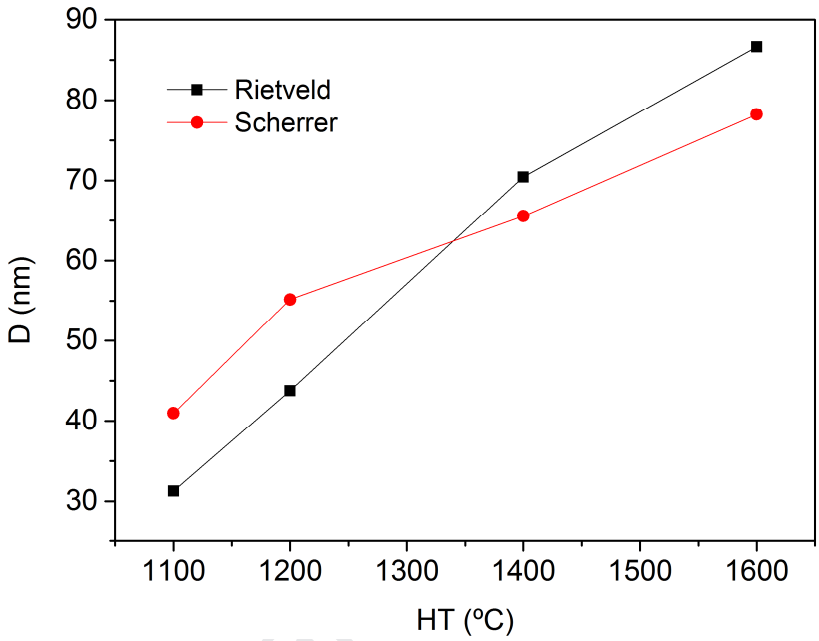

Figure 3 - Treatment temperature dependence of the $ErNbO_4$ average crystallite size, calculated from Rietveld fitting and Scherrer's formula.

STEM analysis was used to further examine the crystallite size and shape for the sample heat-treated at 1600 ºC, since this is the sample with the most promising dielectric properties, as it will be shown later.

Figure 4 displays the STEM bright field micrographs of the powders treated at 1600 ºC, where it can be seen that the morphology of the $ErNbO_4$ crystals is approximately oval.

The crystallite size distribution and abundance is shown in figure 5. The average crystallite size obtained was 81.74 nm, from what we can see a good agreement with the results previously obtained from the XRD measurements, in particular for the Scherrer's formula.

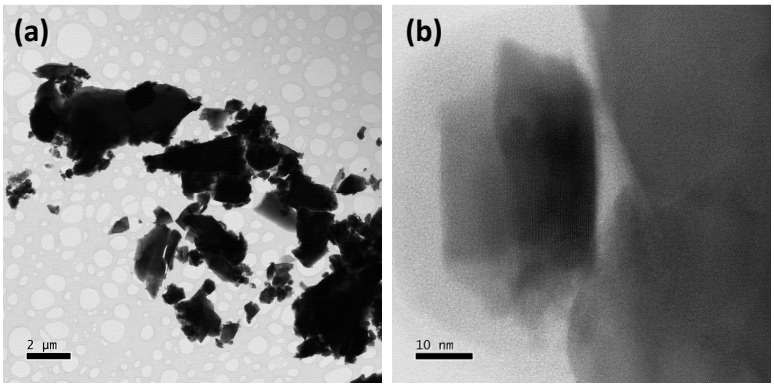

Figure 4 – (a) STEM and **(b)** high resolution STEM micrographs of the sample heat-treated at 1600 ºC.

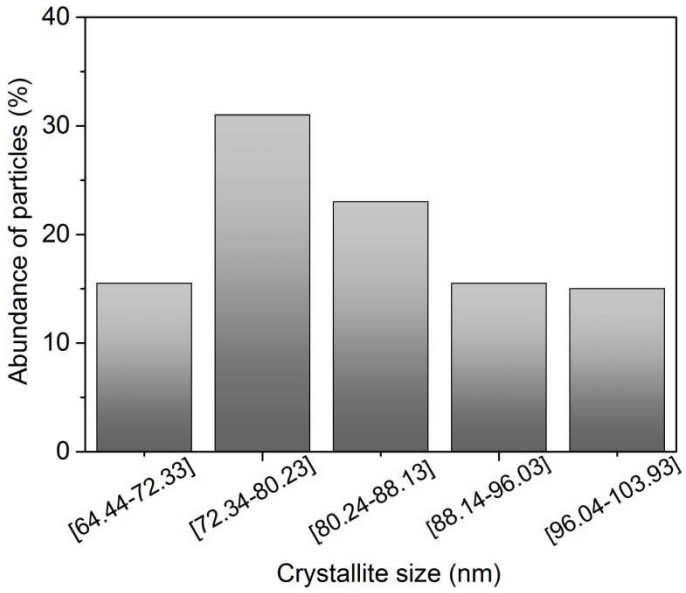

Figure 5 – Crystallite size distribution and abundance in the sample heat-treated at 1600 ºC.

Figure 6 shows the STEM-EDX mapping analysis of the same sample, where the homogeneous distribution of Er, Nb and O elements on the surface of the particles can be seen. Furthermore, no impurities were detected.

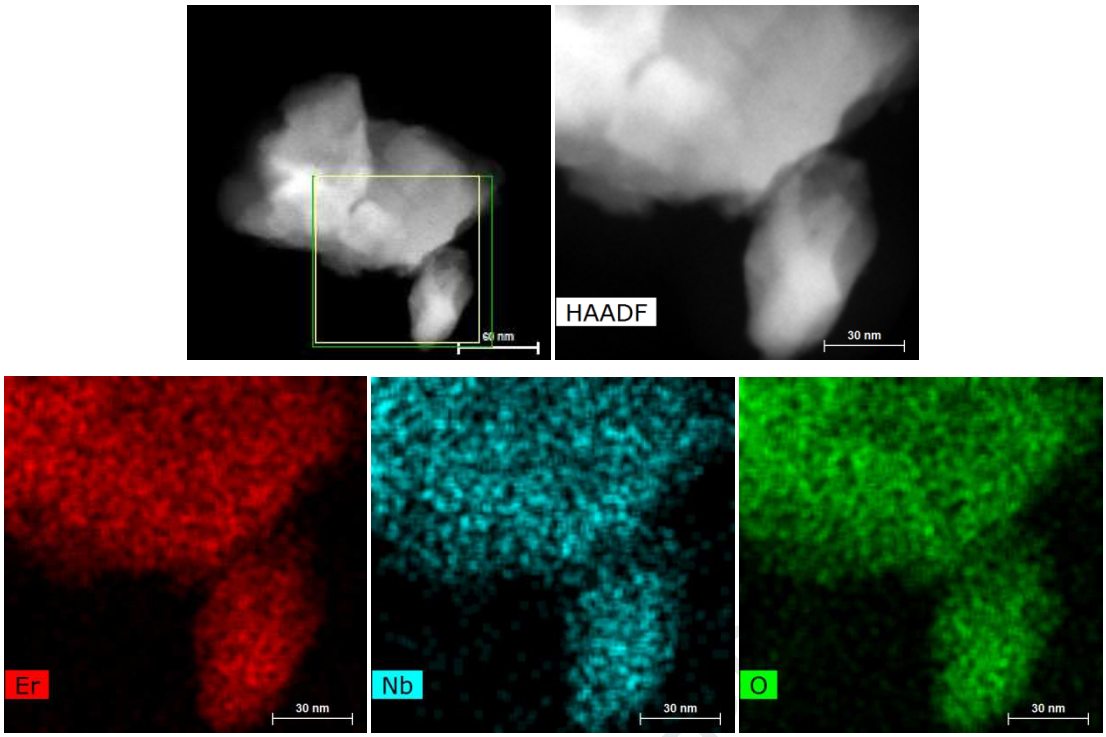

Figure 6 - STEM-EDX mapping analysis of the sample heat-treated at 1600 ºC.

The values of theoretical density, ρ_{theo}, bulk density, ρ_{exp}, fractional porosity, P, and the unit cell volume, V_{cell}, were obtained by the following equations [31-33].

$$\rho_{theo} = \frac{ZM}{N_A V_{cell}} \quad (5)$$

$$V_{cell} = a\,b\,c\sin\beta \quad (6)$$

$$\rho_{exp} = \frac{m}{\pi r^2 h} \quad (7)$$

$$P = 1 - \frac{\rho_{exp}}{\rho_{teo}} \quad (8)$$

where Z and V_{cell} are the number of atoms and the volume of a unit cell, respectively, M is the molar mass, N_A is Avogadro's constant, a, b, c and β are the lattice constants, m is the mass of the cylindrical samples, r and h are the radius and the high of the cylinders, respectively.

The volumes of the unit cells were calculated using the data obtained from the Rietveld refinement and the number of atoms in a unit cell in $ErNbO_4$ is 4 [21].

The results are summarized in Table II.

Table II - Theoretical density, ρ_{theo}, bulk density, ρ_{exp}, and porosity, *P*.

HT (ºC)	1100	1200	1400	1600
ρ_{theo} (g cm^{-3})	7.40	7.41	7.40	7.40
ρ_{exp} (g cm^{-3})	4.13	5.00	5.53	6.55
P (%)	44	32	25	11

The values of the theoretical density remain approximately constant with the increase of the treatment temperature and the results show that the heat-treatment promotes the increase of the bulk density and, consequently, the decrease of the porosity.

Raman spectroscopy was made and the resultant spectra are shown in figure 7(a). The Raman spectra of the samples with single phase $ErNbO_4$ are consistent, with very small variations of intensity and position of the Raman peaks. In Figure 7(b) is shown, in more detail, the Raman spectrum of the sample treated at 1600 ºC. Similarly to the other samples with single phase $ErNbO_4$, HT1600 possess peaks centred at 128, 184, 197, 228, 238, 330, 340, 427, 445, 474, 500, 520, 547, 662, 676, 701, 707 and 814 cm^{-1}. Sixteen of the eighteen peaks identified in these six samples were already associated in literature to monoclinic $ErNbO_4$ [6,34]. The peaks occurring at 520 and 547 cm^{-1} had not been yet assigned to $ErNbO_4$.

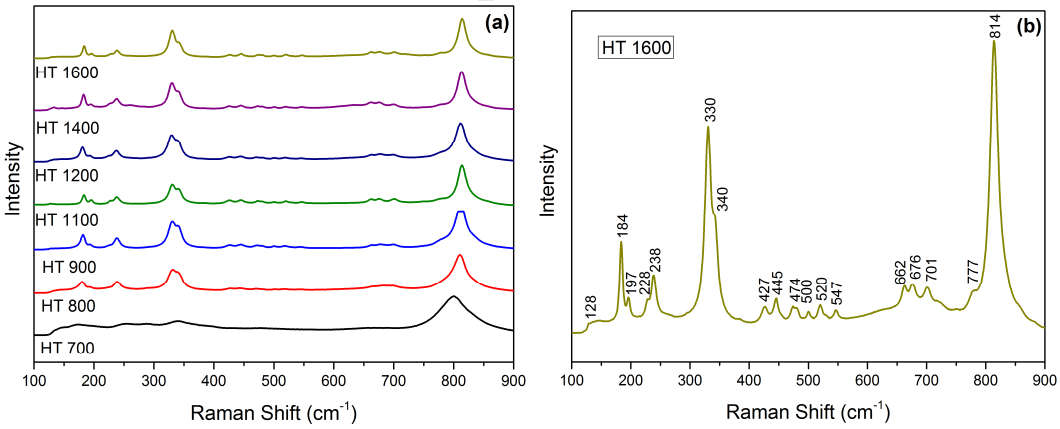

Figure 7 – (a) Raman spectra of the prepared powders; **(b)** Raman spectra of the HT 1600 sample.

SEM micrographs, showed in figure 8, reveal the morphology changes with the increase of the treatment temperature, for the samples with single $ErNbO_4$ phase. As it was expected, the size of the grains increased with the heat-treatment temperature from approximately 0.5 µm (sample HT1100) to more than 10 µm (sample HT1600). Regarding the grains form, they have a prismatic habit being in agreement with the literature [35]. Analysing the surface and fracture of the sample HT1200 it is visible the similar grain size, confirming that the time of sinterization

was enough to keep the same morphology either inside and on the surface of the sample. This similarity between the grain size inside and on the surface, was observed for all the samples.

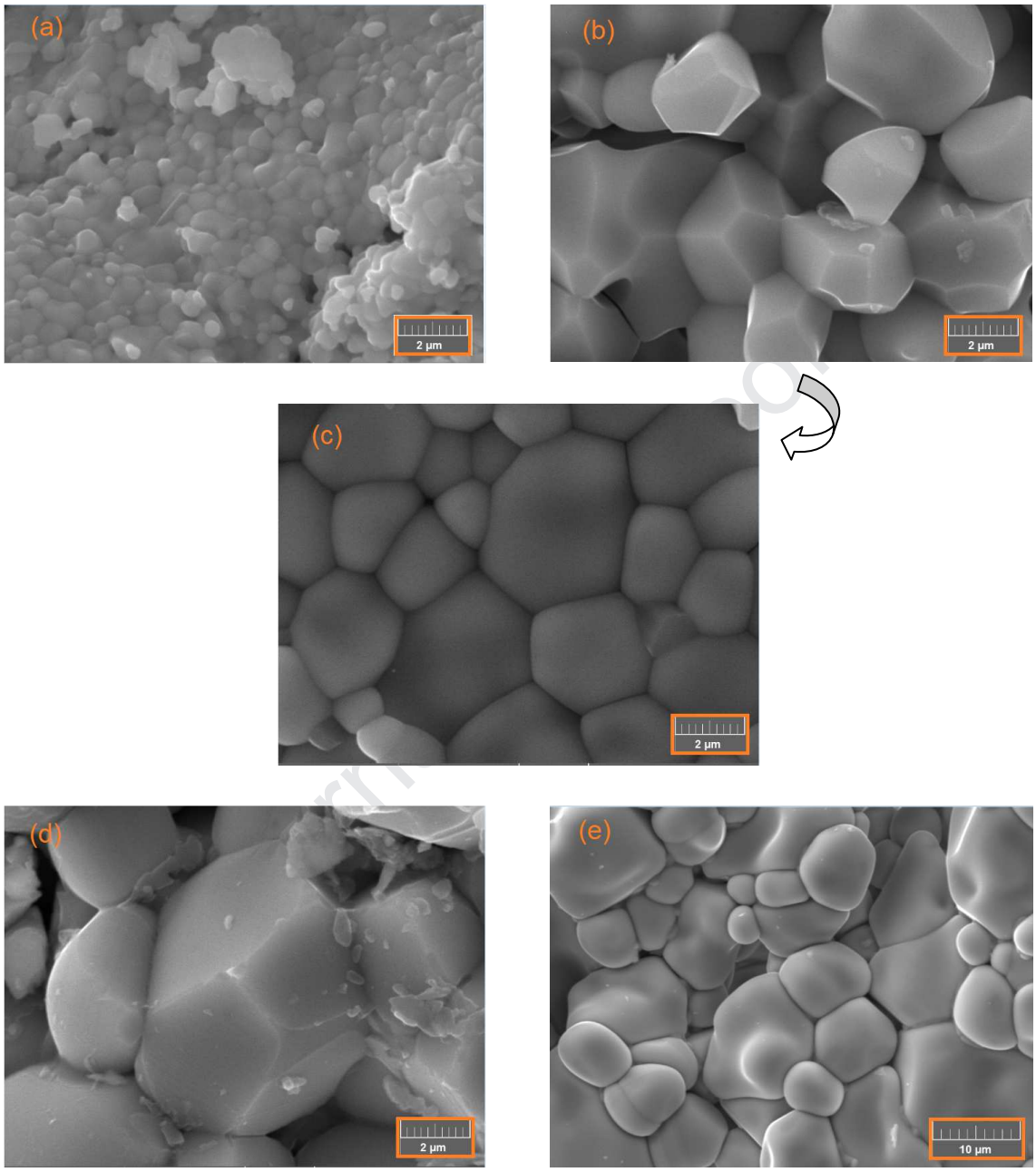

Figure 8 – SEM micrographs of the samples **(a)** HT1100, **(b)** HT1200, **(d)** HT1400, **(e)** HT1600 surfaces and **(c)** HT1200 fracture.

In figure 9(a) is presented the measured transmission of the 2.7 GHz cavity, for the cavity with the sample holder, the sample holder filled with PTFE and filled with the sample treated at 1600 ºC, where the shift in the resonant frequency of the cavity, Δf, is observed. Figure 9(b) shows the real part of the complex permittivity, as function of the treatment temperatures, where one

can notice that the dielectric constant increases with the increase of the treatment temperature. Table III summarizes the ε' and ε'' values, obtained for the different samples, at room temperature.

Analyzing the samples with single phase (the ones treated from 1100 up to 1600 ºC), it can be seen that the dielectric constant increases, as expected, with the decrease of the fractional porosity. The ε'' values are in the range of 0.04 and 0.11, with the highest value occurring for the sample treated at 1200 ºC.

Comparing the samples with single $ErNbO_4$ with the samples where secondary phases were identified, it is detectable an increase in the dielectric constant values, however, without significant increases in the losses.

Considering only the samples where single $ErNbO_4$ was obtained, one can see that the samples with lower ε'' are, as expected, the samples with higher bulk density/lower fractional porosity, i.e., the samples treated at 1400 and 1600 ºC.

In addition to the losses due to porosity, and even in a fully dense ceramic, the grain boundaries can also be the source of losses, since that is not present in a single crystal.

It was expected that the increase of the crystallite size promoted a decrease of ε'' values, since the number of grain boundaries decrease with the increase of the crystallite size. Analyzing these two parameters, one can see that for the samples treated at 1100 and 1200 ºC, ε'' remained approximately constant, regardless of the variation in the crystallite size. The heat-treatment preformed at 1400 ºC promoted a decrease in the ε'' value, which remained constant with the treatment of 1600 ºC, despite the increase in the crystallite size. This not unprecedented but unexpected relation, can be due to the fact that bulk density also varied significantly, making a firm correlation between crystallite size and dielectric properties unpredictable [36-38].

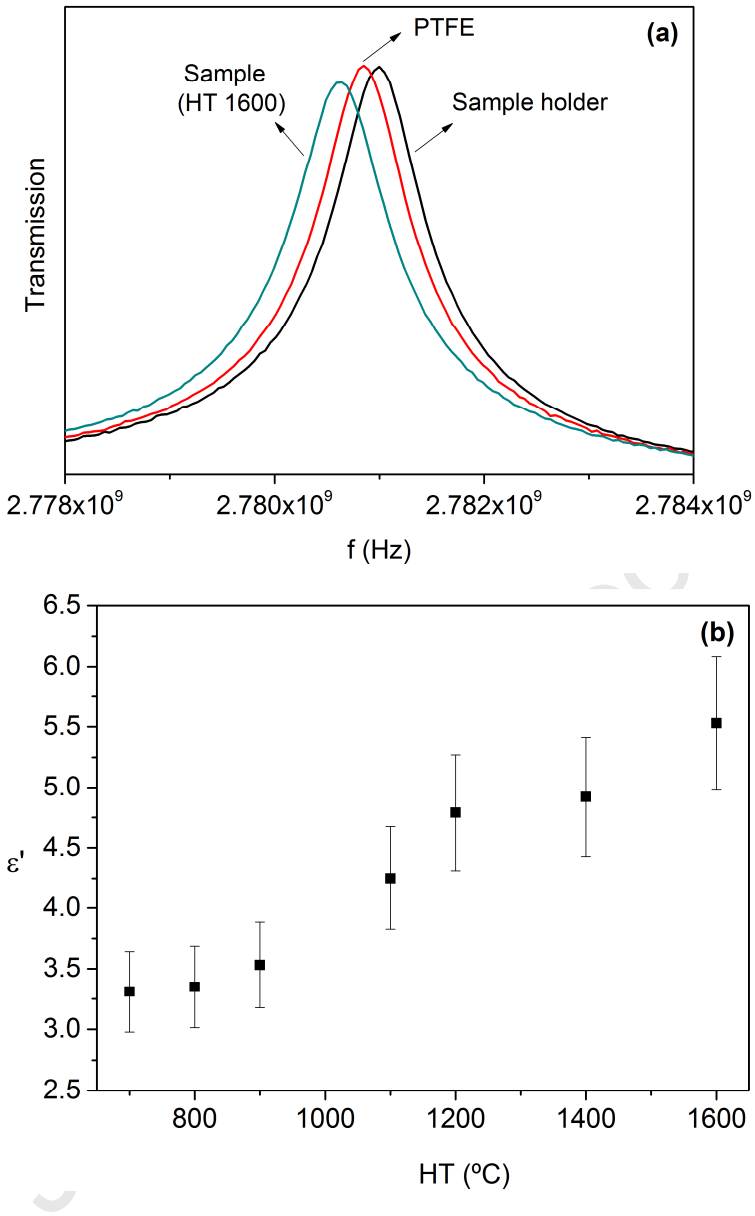

Figure 9 - (a) Measured transmission of the 2.7 GHz cavity; **(b)** Calculated ε' as function of treatment temperature, at 2.7 GHz and 300 K.

Table III - Calculated ε' and ε'' for the different samples, at 2.7 GHz and 300 K.

HT (ºC)	700	800	900	1100	1200	1400	1600
ε'	3.31	3.35	3.53	4.25	4.79	4.92	5.53
ε''	0.08	0.07	0.04	0.10	0.11	0.07	0.07

The variation of ε' has been studied using models that consider the dielectrics as a composite system of two dielectrics with different dielectric constants, being one of the phases the porosity, with ε' = 1 [36].

Heidinger *et al.*[39] proposes the following general relation for spherical pores in a dielectric

$$1-\mathrm{P}=\left(\frac{\varepsilon_{\mathrm{d}}^{'}}{\varepsilon'}\right)^{1/3}\frac{\varepsilon'-1}{\varepsilon_{\mathrm{d}}^{'}+1} \tag{9}$$

where $\varepsilon_{d}^{'}$ is, in this case, and considering the heat treatments from 1100 ºC, the dielectric constant of $ErNbO_4$.

Since equation (9) has no analytical solution in terms of ε', Heidinger *et al.* [39] suggests a linearized approximation for $\varepsilon_{\mathrm{d}}^{'}-\varepsilon'<<\varepsilon_{\mathrm{d}}^{'}$,

$$\varepsilon'=\varepsilon_{d}^{'}\left(1-\frac{3P\left(\varepsilon_{d}^{'}-1\right)}{2\varepsilon_{d}^{'}+1}\right) \tag{10}$$

The dielectric permittivity plotted with respect to fractional porosity, for the samples with single phase, can be seen in Figure 10. The y-intersect of the fitted line, 5.95, represents the dielectric constant $\varepsilon_{d}^{'}$, in other words, an estimated value for the dielectric constant of $ErNbO_4$ in a zero porosity sample case, which is not much different of the ε' value obtained for the sample treated at 1600 ºC.

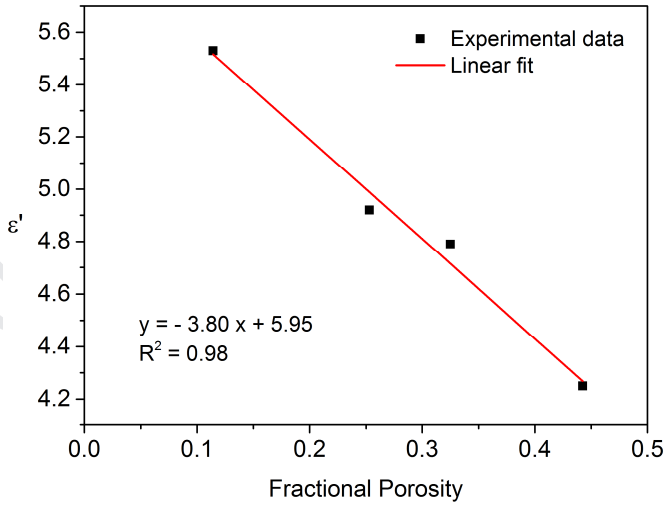

Figure 10 - Fractional porosity dependence of $ErNbO_4$ samples dielectric constant.

4 Conclusions

The $ErNbO_4$ ceramic powders were prepared successfully by the sol-gel method, with the single phase $ErNbO_4$ formed at treatment temperatures from 1100 up to 1600 °C.

The crystallite size was estimated through the Rietveld refinement method and through the Scherrer's formula, with the two processes presenting consistent results.

The dielectric study revealed that the real part of the complex permittivity increases with the increase of the treatment temperature, with the imaginary part of the complex permittivity presenting values in the range of 0.04 and 0.11.

The Heidinger *et al.* [39] model was applied, showing that the estimated value for the dielectric constant of $ErNbO_4$ in a zero porosity sample case is 5.95, not much higher than the one calculated for the sample treated at 1600 ºC.

Acknowledgment

This work is funded by FEDER funds through the COMPETE 2020 Programme and National Funds through FCT - Portuguese Foundation for Science and Technology under the project UID/CTM/50025/2019.

This work was partially supported by Horizon 2020 ASCENT EU project (Access to European Nanoelectronics Network – Project n.º 654384).

The authors acknowledge the post-doctoral grant under the project "SUSpENsE -CENTRO-01-0145-FEDER-000006".

References

[1] S. Butee, A. Kulkarni, O. Prakash, R. Aiyar, K. Sudheendran, K. Raju. "Effect of lanthanide ion substitution on RF and microwave dielectric properties of $BiNbO_4$ ceramics", *J. Alloy. Compd.*, 492(1-2), 351-357, 2010.

[2] Z. Zhang, Y. Tang, H. Xiang, A Yang, Y Wang, C Yin, Y. Tian. "$Li_5Ti_2O_6F$: a new low-loss oxyfluoride microwave dielectric ceramic for LTCC applications", *J. Mater. Sci.*, 55(1), 107-115, 2020.

[3] A. Raveendran, M. T. Sebastian, S. Raman. "Applications of microwave materials: A review". *J. Electron. Mater.*, 48(5), 2601-2634, 2019.

[4] D. Zhou, L. Pang, H. Wang, X. Yao. "Phase composition and phase transformation in $Bi(Sb,Nb,Ta)O_4$ system". *Solid State Sci.*, 11(11), 1894-1897, 2019.

[5] A. Sales, P. Oliveira, J. Almeida, M. Costa, H. Rodrigues, A. Sombra. "Copper concentration effect in the dielectric properties of $BiNbO_4$ for RF applications". *J. Alloy. Compd.*, 542, 264-270, 2012.

[6] K. P. Siqueira, R. L. Moreira, A. Dias. "Synthesis and crystal structure of lanthanide orthoniobates studied by vibrational spectroscopy". *Chem. Mater.*, 22(8), 2668-2674, 2010.

[7] P. Hajra, S. Kundu, A. Maity, C. Bhattacharya. "Facile photoelectrochemical water oxidation on Co^{2+} - adsorbed $BiVO_4$ thin films synthesized from aqueous solutions". *Chem. Eng. J.*, *374*, 1221-1230, 2019.

[8] K. Dzierzgowski, S. Wachowski, M. Gazda, A. Mielewczyk-Gryń. "Terbium Substituted Lanthanum Orthoniobate: Electrical and Structural Properties". *Crystals*, 9(2), 91, 2019.

[9] R. Radha, U. N. Gupta, V. Samuel, H. Muthurajan, H. H. Kumar, V. Ravi. "A co-precipitation technique to prepare $BiNbO_4$ powders". *Ceram. Int.*, 34(6), 1565-1567, 2008.

[10] C. G. Almeida, H. M. C. Andrade, A. J. S. Mascarenhas, L. A. Silva. "Synthesis of nanosized β-$BiTaO_4$ by the polymeric precursor method". *Mater. Lett.*, 64(9), 1088-1090, 2010.

[11] H. F. Zhai, X. Qian, J. Z. Kong, A. D. Li, Y. P. Gong, H. Li, D. Wu. "Abnormal phase transition in $BiNbO_4$ powders prepared by a citrate method". *J. Alloys Compd.*, 509(42), 10230-10233, 2011.

[12] H. F. Zhai, A. D. Li, J. Z. Kong, X. F. Li, J. Zhao, B. L. Guo, J. Yin, Z. S. Li. "Preparation and visible-light photocatalytic properties of $BiNbO_4$ and $BiTaO_4$ by a citrate method". *J. Solid State Chem.*, 202, 6-14, 2013.

[13] N. Wang, M. Y. Zhao, Z. W. Yin. "Low-temperature synthesis of β-$BiNbO_4$ powder by citrate sol–gel method". *Mater. Lett.*, 57(24-25), 4009-4013, 2003.

[14] Y. Dan, H. Xu, Y. Zhang, K. Zou, Q. Zhang, Y. Lu, G. Chang, Q. Zhang, Y. He. "High-energy density of $Pb_{0.97}La_{0.02}(Zr_{0.50}Sn_{0.45}Ti0.0_5)O_3$ antiferroelectric ceramics prepared by sol-gel method with low-cost dibutyltin oxide". *J. Am .Ceram. Soc.*, 102(4), 1776-1783, 2019.

[15] S. Devesa, M. P. Graça, L. C. Costa. "Structural, morphological and dielectric properties of $BiNbO_4$ ceramics prepared by the sol-gel method". *Mater. Res. Bull.*, 78, 128-133, 2016.

[16] S. Narang, S. Bahel. "Low loss dielectric ceramics for microwave applications: a review". *J. Ceram. Process. Res.*, 11(3), 316-321, 2010.

[17] P. Sarin, R. W. Hughes, D. R. Lowry, Z. D. Apostolov, W. M. Kriven. "High-Temperature Properties and Ferroelastic Phase Transitions in Rare-Earth Niobates ($LnNbO_4$)". *J. Am. Ceram. Soc.*, 97, 3307-3319, 2014.

[18] D. W. Kim, D. K. Kwon, S. H. Yoon, K. S. Hong, "Microwave dielectric properties of rare-earth ortho-niobates with ferroelasticity". *J. Am. Ceram. Soc.*, 89, 3861-3864, 2006.

[19] N. Wang, M. Zhao, Z. Yin. "Effects of Ta_2O_5 on microwave dielectric properties of $BiNbO_4$ ceramics". *Mater. Sci. and Eng. B*, 99(1-3), 238-242.

[20] S. Devesa, S. Soreto, M. P. Graça, L. C. Costa, Design. "Characterization and Test Performances of a Resonant Cavity for Complex Permittivity Measurements Using the Small Perturbation Technique", in *Electrical Measurements: Introduction, Concepts and Applications*, Nova Science Publishers, 2018.

[21] G. J. McCarthy. "X-ray studies of $RENbO_4$ compounds". *Acta Crystallogr., Sect. B: Struct. Sci.*, 27(11), 2285-2286, 1971.

[22] B. Toby. "R factors in Rietveld analysis: how good is good enough?". *Powder Diffr.*, 21(1), 67-70, 2006.

[23] A. K. Zak, W. A. Majid, M. E. Abrishami, R. Yousefi. "X-ray analysis of ZnO nanoparticles by Williamson–Hall and size–strain plot methods". *Solid State Sci.*, 13(1), 251-256, 2011.

[24] V. D. Mote, Y. Purushotham, B. N. Dole. "Williamson-Hall analysis in estimation of lattice strain in nanometer-sized ZnO particles". *J. Theor. Appl. Phys.*, 6(1), 1-8, 2012.

[25] A. Patterson. "The Scherrer Formula for X-Ray Particle Size Determination". *Phys. Rev.*, 56 (10), 978-982, 1939.

[26] F.W. Jones. "The measurement of particle size by the X-ray method". *Proc. Roy. Soc. A*, 166(924), 16-43, 1938.

[27] K. Rao, S. Buddhudu. "Structural, Thermal and Dielectric Properties of $BiNbO_4$ Ceramic Powder". *Ferroelec. Lett. Sect.*, 37(6), 101-109, 2010.

[28] D. Zhang, G. Lan, X. Chen, D. Zhu. "X-ray diffraction study on precipitate of Er: $LiNbO_3$ induced by vapor transport equilibration". *Appl. Phys. A*, 74(2), 265-272, 2002.

[29] A. F. L. Almeida, P. B. A. Fechine, M. P. F. Graça, M. A. Valente, A. S. B. Sombra. "Structural and electrical study of $CaCu_3Ti_4O_{12}$ (CCTO) obtained in a new ceramic procedure". *J. Mater. Sci.-Mater. Electron.*, 20(2), 163-170, 2009.

[30] O. M. Lemine, M. Sajieddine, M. Bououdina, R. Msalam, S. Mufti, A. Alyamani. "Rietveld analysis and Mössbauer spectroscopy studies of nanocrystalline hematite α-Fe_2O_3". *J. Alloy. Compd.*, 502(2), 279-282, 2010.

[31] M. J. Iqbal, M. N. Ashiq, I. H. Gul. "Physical, electrical and dielectric properties of Ca-substituted strontium hexaferrite ($SrFe_{12}O_{19}$) nanoparticles synthesized by co-precipitation method". *J. Magn. Magn. Mater.*, 322(13), 1720-1726, 2010.

[32] P. Jéhanno, M. Heilmaier, H. Kestler. "Characterization of an industrially processed Mo-based silicide alloy". *Intermetallics*, 12(7), 1005-1009, 2004.

[33] C. Kittel. "Elementary solid state physics: a short course". Wiley, 1962.

[34] D. L. Zhang, P. R.Hua, E. Yue-Bun Pun, G. G. Siu. "X-Ray, Micro-Raman, Optical Absorption/Emission Studies of $ErNbO_4$ Grown by Vapor Transport Equilibration". *J. Am. Ceram. Soc.*, 90(9), 2893-2899, 2007.

[35] C. Nico. “Niobium Oxides and Niobates Physical Properties”, PhD Thesis, University of Aveiro, Portugal, 2015.

[36] S. J. Penn, N. M. Alford, A. Templeton, X. Wang, M. Xu, M. Reece, K. Schrapel. "Effect of porosity and grain size on the microwave dielectric properties of sintered alumina". *J. Am. Ceram. Soc.*, 80(7), 1885-1888, 1997.

[37] K. V. R. Prasad, A. R. Raju, K. B. R. Varma. "Grain size effects on the dielectric properties of ferroelectric $Bi_2VO_{5.5}$ ceramics". *J. Mater. Sci.*, 29(10), 2691-2696, 1994.

[38] D. M. Iddles, A. J.Bell, A. J. Moulson. "Relationships between dopants, microstructure and the microwave dielectric properties of ZrO_2-TiO_2-SnO_2 ceramics". *J. Mater. Sci.*, 27(23), 6303-6310, 1992.

[39] R. Heidinger, S. Nazare. "Influence of porosity on the dielectric properties of AlN in the range of 30- 40 GHz". *Powder Metall. Int.*, 20(6), 30-32, 1988.

Highlights

- $ErNbO_4$ ceramic powders were successfully prepared by the sol-gel method;
- A relation between the crystallite size and the lattice strain estimated through the Rietveld analysis was established;
- The crystallite size of $ErNbO_4$ was obtained by three different methods, Rietveld refinement, Scherrer's formula and STEM analysis, with the results showing a good consistency;
- The dielectric constant of $ErNbO_4$ in a zero porosity sample case was estimated and one can conclude that this value is not much higher than the dielectric constant obtained for the sample treated at 1600 ºC;
- The dielectric constant increases with the increase of the treatment temperature, without significant increases of the losses.

Declaration of interests

× The authors declare that they have no known competing financial interests or personal relationships that could have appeared to influence the work reported in this paper.

☐The authors declare the following financial interests/personal relationships which may be considered as potential competing interests: